Available online at www.sciencedirect.com

SciVerse ScienceDirect

Ceramics International 39 (2013) 3141–3149

CERAMICS INTERNATIONAL

www.elsevier.com/locate/ceramint

Synthesis and mechanical characterization by nanoindentation of polycrystalline YAG with Eu and Nd additions

D. Lozano-Mandujano[a], J. Zárate–Medina[b], R. Morales-Estrella[b], J. Muñoz-Saldaña[a,*]

[a]*Centro de Investigación y de Estudios Avanzados del IPN, Materials Science and Engineering, Unidad Queretaro, Libramiento Norponiente No. 2000, Fracc. Real de Juriquilla, Queretaro, Qro., CP 76230, México*

[b]*Instituto de Investigaciones Metalúrgicas, UMSNH, Av. Universidad No. 1600, Morelia, Mich., CP 58060, México*

Received 2 July 2012; received in revised form 16 September 2012; accepted 27 September 2012
Available online 7 October 2012

Abstract

Mechanical properties measured by nanoindentation of ceramics of pure YAG, as well as doped with 2 and 5 at% Eu and Nd synthesized by a modification of the Pechini-type precursor method that includes the formation of spherical agglomerates by spray drying, are reported. The densification of sintered doped samples was successfully achieved at temperatures as low as 1550 °C in air using nanometric-sized powders produced by high-energy ball milling. A slight increase in the lattice parameter due to Eu and Nd additions to the YAG was observed, as expected, but effectively no change in mechanical properties was observed. Within the standard deviation, the hardness was 22 GPa and the elastic modulus was 315 GPa for all samples. These values are more than twice as large as those previously reported for amorphous fibers prepared with the same compositions but similar to literature reports for single crystals.

Keywords: Milling; Sintering; Mechanical properties; YAG

1. Introduction

Ceramics based on alumina doped with rare-earth oxides have several properties that make them very attractive for a range of applications [1–3]. Particularly, the combination of aluminum oxide and yttrium oxide in stoichiometric proportions forms compounds called yttrium aluminum garnets (YAG), which are suitable for applications in the electronic industry, such as solid-state lasers [4]. The unit cell of YAG consists of a complex body-centered-cubic lattice (space group Ia3d) with a lattice parameter of ~1.2 nm [2].

Polycrystalline pure YAG or in the form of composites has many potential applications as a high-temperature engineering material [5]. The alumina-YAG system in the eutectic composition has been identified as an ultra-high-temperature structural material [3]. Several studies in the past decade have confirmed the superior mechanical properties of this eutectic system at temperatures above 1400 °C [1]. Simultaneous with these developments, a survey of the creep resistance of single crystal oxides was performed, including YAG, one of the most commonly used [6]. The high creep resistance of YAG is attributed to the large lattice parameter and hence large Burgers vector of the dislocations [7–9].

To obtain YAG powders, various methods have been employed, including precipitation of hydroxides [10–12], sol–gel processes [13–15], urea method [16], spray pyrolysis [17], combustion synthesis [18], and citrate gel [19], among others. However, the most traditional is still the mixed-oxides method assisted by high-temperature solid-state synthesis. This method has the disadvantage of using high temperatures (~1600 °C) as well as long processing times.

The "citrate precursor" or Pechini method has been used elsewhere for the synthesis of YAG [19]. Lower processing temperatures (900 °C) are achieved and material homogenization is improved by using rare earth elements as dopants. A modified citrate precursor method was reported previously by J. Zarate, et al. [20], who described the production of a completely pure YAG phase with significant reduction of the processing time compared to the normal route of citrate precursor. An additional

*Corresponding author. Tel.: +52 442 2119924; fax: +52 442 2119938.
E-mail address: jmunoz@qro.cinvestav.mx (J. Muñoz-Saldaña).

0272-8842/$ - see front matter
http://dx.doi.org/10.1016/j.ceramint.2012.09.095

advantage of this modified synthesis route, compared with other techniques, is that a better distribution of yttrium and aluminum ions is achieved in the mixture. The reason for the homogenous conditions is due to a spray-drying step, which renders a high degree of dispersion of salts and organics with a short effective diffusion distance. Thus, once the organics are removed, the ions remain homogeneously distributed, which leads directly to a decrease in the processing temperature of YAG compared to previous results reported in the literature [21,22].

Mechanical characterization of dense YAG material, particularly of intrinsic properties such as elastic modulus, is relevant because YAG is often used as a reinforcement phase in ceramics. Nanoindentation offers a set of techniques, which despite the small size of an indentation imprint, is a well-established methodology for the characterization of mechanical properties of bulk materials (metals, ceramics), thin films, amorphous solids, fibers, etc. [23]

The objective of this work was to evaluate, using nanoindentation, the mechanical properties of Nd- and Eu-doped crystalline YAG synthesized by the modified citrate precursor route. The results are compared with previously reported mechanical properties of amorphous YAG fibers with the same composition.

2. Materials and methods

Aluminum nitrate (99.9% J.T. Baker), yttrium nitrate (99.9% Aldrich), europium and neodymium oxides (99.99% Alpha-Aesar), citric acid (J.T. Baker), ethylene glycol (99.9% J.T. Baker) and deionized water were used as raw materials. Solutions with compositions corresponding to YAG, YAG:Eu 2at%, YAG:Eu 5at%, YAG:Nd 2at%, and YAG:Nd 5at% were prepared by a modification of the Pechini-type precursor method as reported by Zarate, et al. [20]. The amount of Eu and Nd additions were relative to the yttrium content in the garnet. To eliminate the solvent and produce precursor powders, the solutions were spray dried (ADL Mini Spray-Dryer 31) using spray pressure, feed rate and temperature of 196 KPa, 0.25 l/h and 180 °C, respectively.

Precursor prepared powders were then calcined in a high-temperature furnace (Thermolyne M46100) at 900 °C for 1 h to promote the crystallization of the YAG phase. YAG calcined powders were uniaxially compacted (95 MPa) for 1 min using an 11-mm diameter piston–cylinder die in a hydraulic press. The amount of powder used for the production of ceramic coupons was 0.35 g. These samples are identified as "spray dried". For mechanical characterization, "spray dried" samples were sintered at 1550 °C for 1 h in air using a heating ramp of 5 °C/min.

To increase the density while keeping the same sintering conditions, a 0.5-h high-energy ball-milling step was added to the processing route using a Retch MM400 mixer mill operated at 25 Hz using 1-cm diameter TZP zirconia balls. This second set of sintered samples is identified as "milled".

The sintered ceramic coupons were characterized by X-ray diffraction using a Rigaku D/Max2100 diffractometer with Co-Kα radiation operated at 30 kV. SEM micrographs (JEOL JSM 5800-LV) were used to estimate the morphology and particle size distribution of the powders and grain size of dense samples. The density of the ceramic coupons was determined by the Archimedes method. Transverse cross-sections were polished with alumina suspensions (particle size of 3 to 0.03 μm) and subsequently with a commercial colloidal silica suspension (Buehler Mastermet II). A slightly "etched" surface was obtained using this polishing procedure.

A Hysitron Ubi1 nanoindentation system with a Berkovich diamond tip and variable load (1000–9000 μN) was used to determine the hardness and reduced elastic modulus on the transverse cross-section of sintered materials. Indentation imprints in a "load control" mode of force versus time were carried out. The system was calibrated by determining compliance, thermal drift (40–60 s), area function, and tip radius using a fused silica reference sample (ASMEC, Germany) as well as point of zero load for all indentation tests.

Compliance was calculated on the basis of the Oliver and Pharr method [24], by making 16 indents at high loads and considering the load frame compliance, C_{frame}.

$$\frac{1}{S_{measured}} = \frac{\sqrt{\pi H}}{2E_{red}}\frac{1}{\sqrt{P_{max}}} + C_{frame} \quad (1)$$

where, $S_{measured}$ is the experimental stiffness, H is the hardness, P_{max} is the maximal applied load and E_{red} is the reduced elastic modulus.

The area function was determined on the basis of 50 indents on a fused silica sample, 25 at "high loads" covering the full range of load (up to 10 mN) and 25 at "low loads", where the maximum load is limited to 2 mN. The area function is calculated on the basis of a polynomial function, following the Oliver and Pharr method [24].

Finally, the tip radius is obtained by approximating of the end of indenter tip to be a sphere and extracting the tip radius from a contact area vs. contact depth curve (using low load indentations, up to 2 mN):

$$A(h_c) = \pi a^2 = -\pi h_c^2 + 2\pi R h_c \quad (2)$$

Atomic force micrographs (AFM) of the "etched" surface were recorded in contact mode using the Berkovich tip as a probe to determine grain size of the dense samples. The limiting factors to characterize by AFM are the surface roughness and densification level. Thus, the average grain size of the "as spray dried" samples was determined only by image analysis of SEM fracture surfaces. Irrespective of the method of determination, cumulative frequency distribution curves as well as a statistical average and standard deviation were obtained.

To evaluate the effect of the milling process route, a Weibull distribution was used to analyze the mechanical properties of the samples (elastic modulus, E_s and hardness, H). In this case, Weibull probability plots help to

organize many different types of data into straight line X–Y plots.

3. Results and discussion

In a previous report [25] additions of 2 and 5 at% Nd and Eu to YAG showed a strong influence on the mechanical behavior of amorphous fibers obtained via a melt extraction process. As mentioned earlier, the main goal of this study was to confirm this effect, but in polycrystalline YAG samples. As shown below, one characteristic of the "milled" samples is that they have a densification level above 96% of the theoretical density, thus avoiding the influence of pore compliance on the experimental elastic modulus. The step-by-step results of the processing route to obtain polycrystalline, high-density samples are presented and discussed below.

Fig. 1 shows typical SEM images of powders of pure YAG and with 5 at% Eu and Nd synthesized by the Pechini method, spray dried and calcined at 900 °C for 1 h. All samples showed spherical agglomerates composed of particles of less than 100 nm, a characteristic previously reported elsewhere [25]. The agglomerate diameters were obtained from a cumulative frequency graphic and are presented in Table 1. The variation observed in these values is fully within the expected behavior for spray drying processes, so that one can conclude that there is no influence of the doping type or contents on the agglomerate size or morphology. The agglomerate size is entirely defined by the spray-drying parameters.

For the densification of the samples, as a first approach, "spray dried" ceramic coupons were prepared directly after the synthesis. The "spray dried" powders were uniaxially pressed and subsequently sintered at 1550 °C in air to promote densification. The sintering temperature of 1550 °C was chosen based on experiments as a function of temperature in the range of 1200–1550 °C.

For the sintered "spray dried" samples the maximum densification measured using the Archimedes method was 85%. To confirm the low densification behavior, the samples were fractured in simple bending. Typical SEM micrographs of the fracture surfaces are shown in Fig. 2. These images confirm the low densification levels. The grain size of the YAG:Eu 2at% sample ranges from 1.0–4.5 μm, whereas the range for the pure YAG, YAG:Eu 5at% and YAG:Nd 2 at% samples is from 0.5–2.0 μm. The YAG:Nd 5at.% lies inbetween. There is no clear connection between dopant content and grain size.

The poor densification behavior was determined by the powder-packing factor obtained in uniaxial pressing. Neither the pressure distribution nor the particle flow during uniaxial pressing were high enough to break the spherical agglomerates obtained by spray drying and calcination. Some variability in densification was observed between samples even though the uniaxial pressure was kept constant. Additionally, it is well known from the literature that there are some difficulties sintering YAG ceramics at the sintering conditions used (1550 °C in air) [26].

Since density is critical, especially in the determination of mechanical properties by nanoindentation, further experiments were carried out in order to increase densification at a maximum sintering temperature of 1550 °C in air. Improvements were achieved by high-energy ball milling the powders just after spray drying but before compacting and sintering. Ball milling of the spray dried and calcined powders was carried out for 30 min, and subsequently the powders were processed in the same manner as the initial samples. The milling time was chosen to minimize contamination. A series of tests performed using the same ball mill and milling parameters, but with pure alumina powder, resulted in 1.82% zirconia (milling media) contamination of

Table 1
Mean particle diameter as a function of dopant concentration.

Sample	Average agglomerate diameter (μm)
YAG	0.51 ± 0.23
YAG:2Eu	0.49 ± 0.36
YAG:5Eu	0.87 ± 0.38
YAG:2Nd	0.60 ± 0.28
YAG:5Nd	0.55 ± 0.28

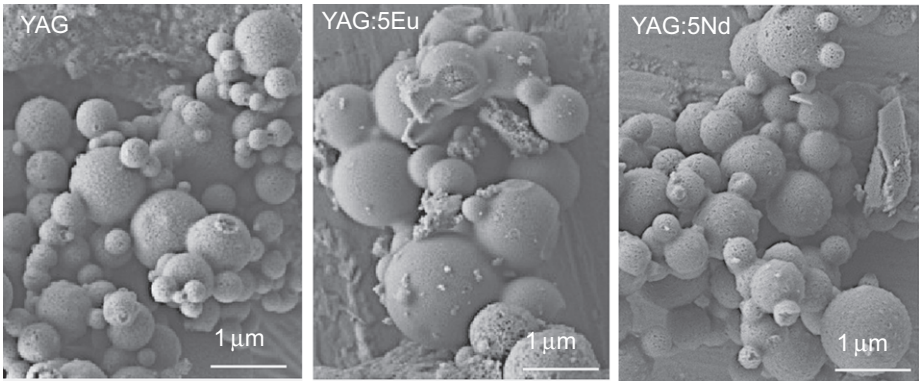

Fig. 1. Typical SEM micrograph of YAG powders, with and without rare-earth additions, processed by spray drying.

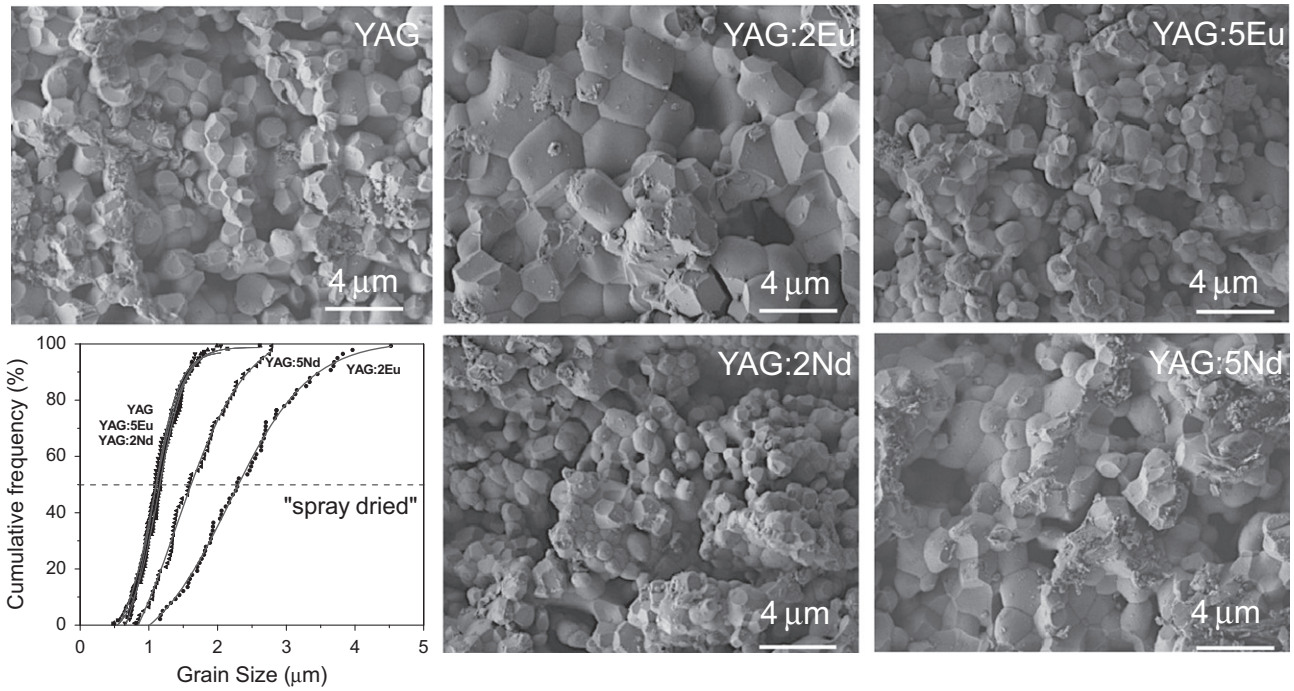

Fig. 2. SEM micrographs of the fracture surface of "spray dried" samples sintered at 1550 °C. The grain size distribution can also be observed.

Table 2
Density as a function of dopant concentration and average grain size of samples sintered at 1550 °C.

Sample	Density (%)	Average grain size (µm)	
	"milled"	"spray dried"	"milled"
YAG	97	1.2 ± 0.2	4.0 ± 0.7
YAG:2Eu	99	2.4 ± 0.4	3.0 ± 0.5
YAG:5Eu	96	1.1 ± 0.2	2.1 ± 0.4
YAG:2Nd	97	1.2 ± 0.2	3.3 ± 0.7
YAG:5Nd	98	1.7 ± 0.3	3.2 ± 0.7

the powder after 30 min of milling. Thus, we can reasonably assume the same purity (98.2%) of the YAG and doped-YAG powder. Table 2 presents the density for all "milled" samples, as well as the average grains size for both the "spray dried" and the "milled" samples. A particle size of less than 100 nm was obtained in the "milled" powder.

Comparing the grain size distribution curves for the "spray dried" samples (Fig. 2) and the "milled" samples (Fig. 3), it can be seen that the additional step of milling resulted in a slight increase in grain size. This observation can also be made by comparing the average values in Table 2. Fig. 3 also includes a typical AFM micrograph of a pure YAG sample in which the grains can be seen more clearly than in the SEM.

X-ray patterns for the compacted and sintered samples are shown in Fig. 4. For all samples, Bragg peaks corresponding to YAG are present, with only very slight differences in peak position and intensity, which indicate again, only slight differences in lattice parameter. This behavior is expected because Eu^{+3} (1.25 Å) and Nd^{+3} (1.12 Å) ions substitute for the smaller Y^{+3} (1.015 Å) ions, resulting in a distortion of the YAG unit cell and a corresponding increase in the lattice parameter (Table 3). The values are in agreement with those of Saladino, et al. [27]. The addition of 2 at% of Eu and Nd expands the cubic lattice of YAG by 0.23% and 0.16%, respectively. The change in size with 5 at% dopant is 0.28% for Eu and 0.30% for Nd. This is consistent with previous findings for Nd-doped YAG, where the reported solubility limit is 12 wt% (16.5 at%) [28].

In order to determine if these changes in lattice parameter are significant, the mechanical properties of the samples were measured. Nanoindentation load-penetration curves (P–h) obtained with a maximum load of 3 mN for "spray dried" and "milled" pure YAG samples are shown in Fig. 5. There, the effect of increasing the densification level due to the milling step can be qualitatively observed in the load-penetration curves, specifically in the hysteris of the loading and unloading curves. In the YAG "milled" samples, in most of the cases the material still shows a fully elastic behavior all the way up to 3 mN.

Fig. 6 shows a comparison of P–h nanoindentation curves made on pure YAG, YAG:Eu 2at% and YAG:Nd 2 at% "milled" samples (a, b and c, respectively). In all cases, the elastic limit can be obtained by applying a Hertzian fit to the indentation loading stage (Fig. 6 a′, b′ and c′). From these images, the onset of plastic deformation for the doped samples is observed at loads around 1.9 mN, which correspond to mean contact pressures (P_m) of ~22 GPa. Pure YAG shows a higher elastic limit, so that the P–h curve doesn't show hysteresis in the unloading stage after 3 mN of applied load. The Hertzian fit also

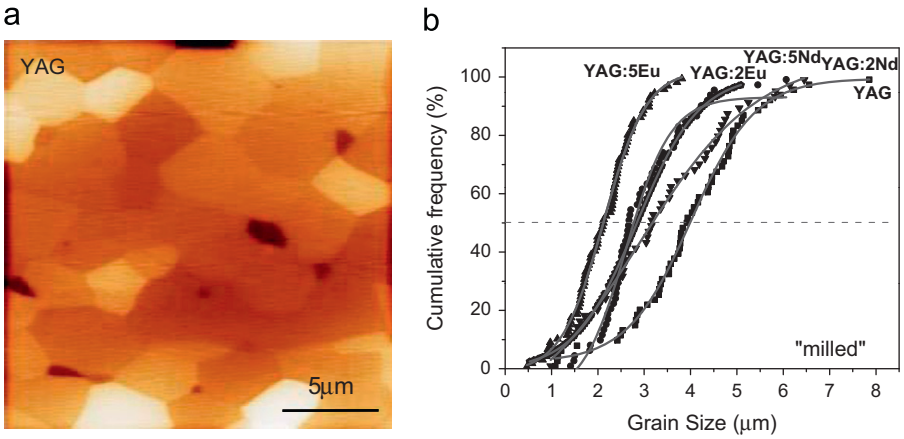

Fig. 3. Effect of the milling step on microstructure: (a) typical AFM micrograph of a pure YAG sample, (b) grain size distribution for all "milled" YAG samples.

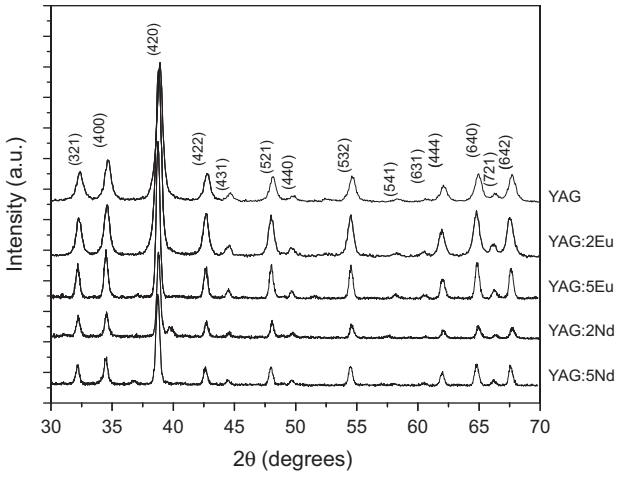

Fig. 4. XRD spectra of samples sintered at 1550 °C.

Table 3
Lattice parameter as a function of dopant concentration of sintered samples.

Sample	Lattice parameter (Å)
YAG	12.014 ± 0.004
YAG:2 Eu	12.042 ± 0.002
YAG:5 Eu	12.048 ± 0.018
YAG:2Nd	12.033 ± 0.016
YAG:5Nd	12.051 ± 0.017

allows the determination of the elastic modulus according to the Hertz equation [29].

$$P = \frac{4}{3} E_{red} R^{1/2} h^{3/2} \tag{3}$$

where P is the maximal load, R is the tip radius (698 nm) and h is the penetration depth.

The indentation hardness (H) and elastic modulus (E_s) were determined from the unloading stage of the P–h curves using the Oliver Pharr method [24]. The Poisson's ratio for YAG, $v=0.23$ [30], was used for all samples in determining the elastic modulus:

$$E_s = \frac{\left(1-v_s^2\right)}{\left(1/E_{red}-\left(1-v_i^2\right)/E_i\right)} \tag{4}$$

where $E_i=1140$ GPa, and $v_i=0.07$ are the elastic constants for the diamond indenter, and E_s and v_s are the elastic constants of the sample. The average values of H and E_s in highly densified ("milled") pure YAG samples are 20.6 ± 1.3 and 319 ± 13 GPa, respectively, which are similar to previously measured values for polycrystalline YAG ($E_S=308$ GPa) [30] The full set of data is presented in Table 4 for "spray dried" samples and Table 5 for "milled" samples.

The calculated values of elastic modulus using the Hertz equation shows an almost perfect match with those calculated by the Oliver & Pharr method (deviations of less than 6%). Another interesting observation that can be made from the results in Tables 4 and 5 is that doping had essentially no effect on the mechanical properties. However, the most glaring observation is the difference in mechanical properties between "spray dried" and "milled" samples. The average elastic modulus of the "spray dried" samples (150 ± 75 GPa) is less than half the average for the "milled" samples (320 ± 13 GPa). Not only that, but the standard deviation is also much larger. These differences are due to compliance resulting from the low density (porosity) of the "spray dried" samples. Although a large standard deviation is an indicator, identifying samples whose low density (porosity) significantly affects their mechanical properties is difficult using traditional methods. Thus, a Weibull analysis of the hardness and elastic modulus data was performed.

Weibull analysis is a technique specialized in the modeling of data exhibiting significant variability, which has been successfully and routinely applied in the analysis of the strength reliability of brittle materials [31] In this work, a two-parameter Weibull model was used to fit the hardness

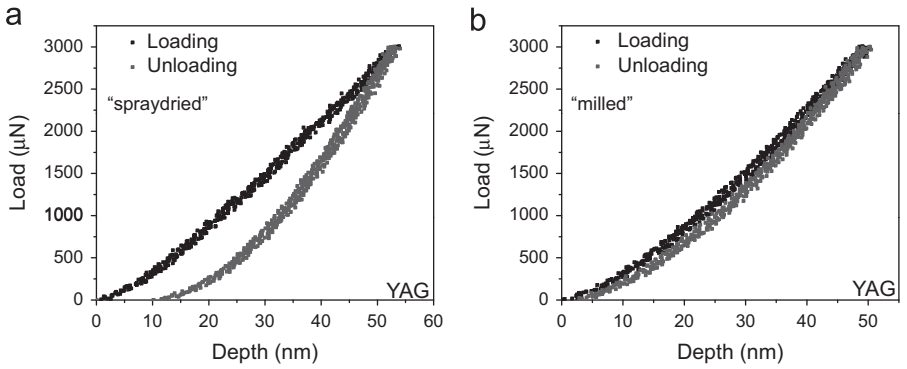

Fig. 5. Comparison of typical nanoindentation curves of "spray dried" and "milled" pure YAG samples.

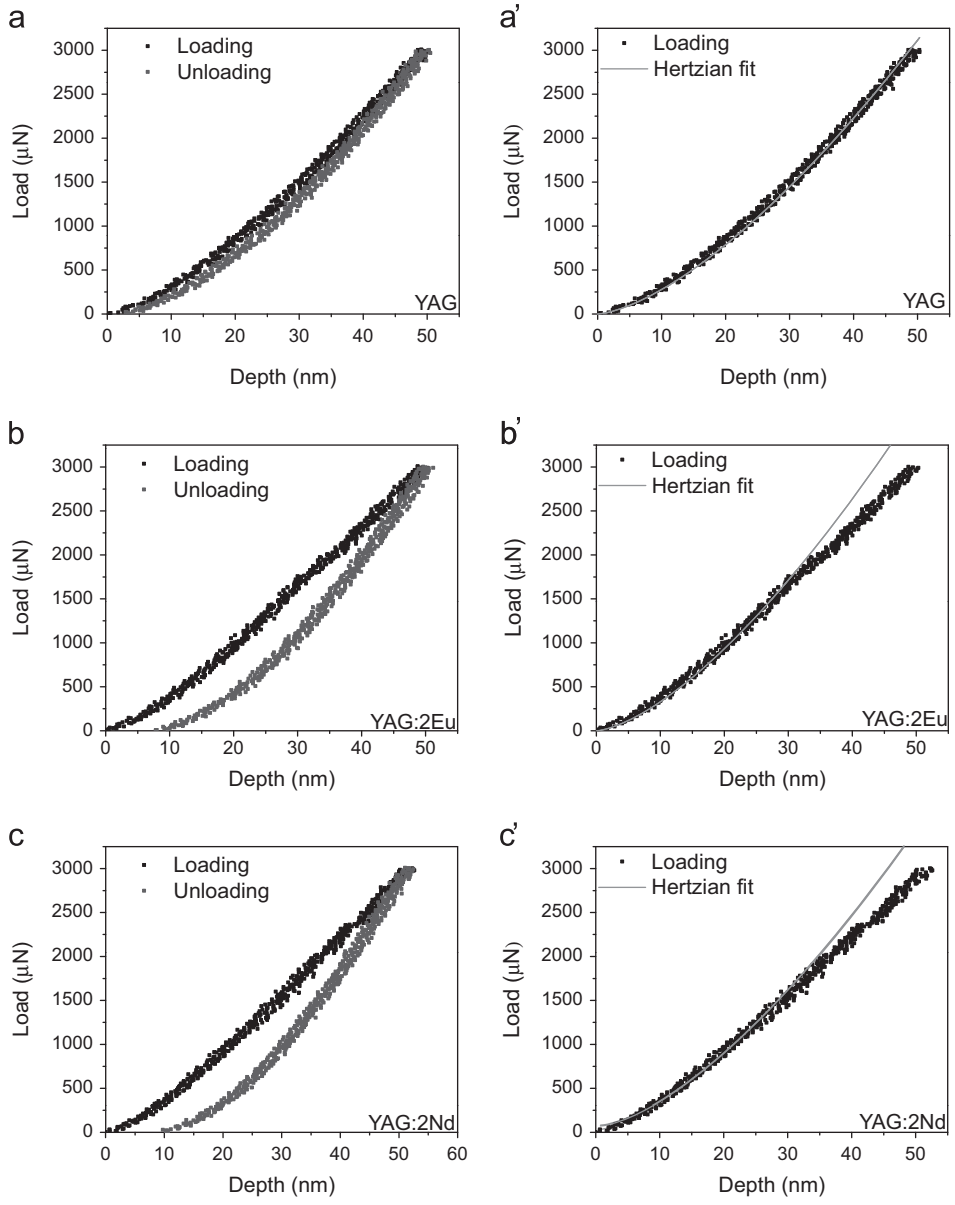

Fig. 6. Comparison of *P–h* nanoindentation curves made for pure YAG, YAG:Eu 2 at% YAG:Nd 2 at% "milled" samples (a, b and c, respectively) and the elastic limit obtained by applying a Hertzian fit to the indentation loading stage (a′, b′ and c′, respectively).

Table 4
Hardness H, elastic modulus E_s, and corresponding Weibull moduli m, along with the values determined by the Oliver & Pharr method for the "spray dried" samples.

Sample	Hardness (GPa)				Elastic modulus (GPa)			
	H	m_1	m_2	$H(O\&P)$	E_s	m_1	m_2	E_s $(O\&P)$
YAG	16.7	1.4	3.4	12.7 ± 7.0	193	2.3	3.3	150 ± 75
YAG:2 Eu	18.3	1.3	3.3	11.3 ± 5.4	237	1.3	3.4	160 ± 75
YAG:5 Eu	15.6	1.6	3.3	11.9 ± 8.1	181	1.8	4.7	120 ± 65
YAG:2Nd	17.5	0.9	2.4	11.2 ± 9.6	132	1.2	3.0	110 ± 85
YAG:5Nd	16.2	0.5	3.5	10.4 ± 5.9	245	0.9	3.8	180 ± 70

Table 5
Hardness H, elastic modulus E_s, and corresponding Weibull moduli m, along with the values determined by the Oliver & Pharr method for the "milled" samples.

Sample	Hardness (GPa)			Eastic modulus (GPa)			Yield (GPa)
	H (*Weibull*)	m (*Weibull*)	H (*O&P*)	E_s (*Weibull*)	m (*Weibull*)	E_s (*O&P*)	P_m (*Hertzian*)
YAG	21.3	23.0	20.6 ± 1.3	327	38.2	319 ± 13	22.1 ± 0.1
YAG:2 Eu	23.5	28.4	23.3 ± 3.0	327	46.8	323 ± 11	22.1 ± 0.3
YAG:5 Eu	21.2	24.2	21.6 ± 2.4	314	46.5	311 ± 11	22.0 ± 0.4
YAG:2Nd	21.1	18.2	20.9 ± 1.9	323	41.7	316 ± 19	22.1 ± 0.1
YAG:5Nd	19.5	27.0	19.5 ± 1.5	330	27.1	313 ± 27	22.1 ± 0.1

and elastic modulus data, based on the equation:

$$p(V) = 1 - \exp\left[-\left(\frac{x}{x_0}\right)^m\right] \quad (5)$$

where p is the probability for the parameter x, V is the volume of interaction, m is the Weibull modulus, a dimensionless quantity, and x_0 is known as the scaling parameter and corresponds to the property of interest (hardness, H, or elastic modulus, E_S). The Weibull data presented in Fig. 7 is based on a modification of Equation (5) by taking the natural logarithm of both sides twice and simplifying:

$$\ln\left[\ln\left(\frac{1}{1-p(V)}\right)\right] = m(\ln(x) - \ln(x_0)) \quad (6)$$

In this case, the Weibull parameter, m, is the slope of the fit, and the Y-intercept yields x_0. The magnitude of m increases as the variability or scatter of the data decreases. As a general rule, when m is greater than 10, the data scatter is considered low [32].

Two observations can be readily made based on inspection of the Weibull plots of Fig. 7. First, all the "spray dried" samples have bimodal distributions with two distinct slopes, which is characteristic of two relatively distinct populations of data. These two populations correspond to differences in density at the nanometric level, where the indentations in higher density areas correspond to the group with higher slope (Weibull parameter m). However, the difference in slope is not significant, as both are small (i.e., the scatter is large) for all the "spray dried" samples, for both hardness and elastic modulus. The values are tabulated in Table 4.

At first consideration, these results may seem negative. However, the low Weibull modulus is a clear indication that the samples are not fully dense, and this determination was made without the need to section the samples. As further confirmation, the scattering of mechanical properties was dramatically reduced by improving the densification of the samples, as evidenced by the much greater slopes ($m = 27$–47). A summary of the hardness and elastic modulus (Weibull-determined and calculated using the Oliver & Pharr method) of the "milled" samples is presented in Table 5. By comparing these results with the values for the "spray dried" samples (from Table 4), it is evident that the dispersion of the experimental data in samples after milling is more than acceptable according to Weibull analyses.

An additional feature can be observed in the hardness Weibull distribution curves. The YAG sample shows a nearly monomodal distribution (almost perfect linear tendency), whereas the doped samples all have bimodal distributions. The smaller group of data mainly shows values with higher hardness. Even for these dense, "milled" samples, there is no evident influence of the type or amount of doping, as the slight variations observed lie within the experimental error (standard deviation), implying that the concentration of dopants used in this work do not alter the mechanical properties of YAG. Table 5. This Table also shows the mean contact pressures calculated using the Hertzian approach for all "milled" samples. There is also no effect of doping on the elastic limit compared to pure YAG, with all values being $\sim$22 GPa.

A similar study of mechanical properites using nanoindentation was recently reported for individual amorphous

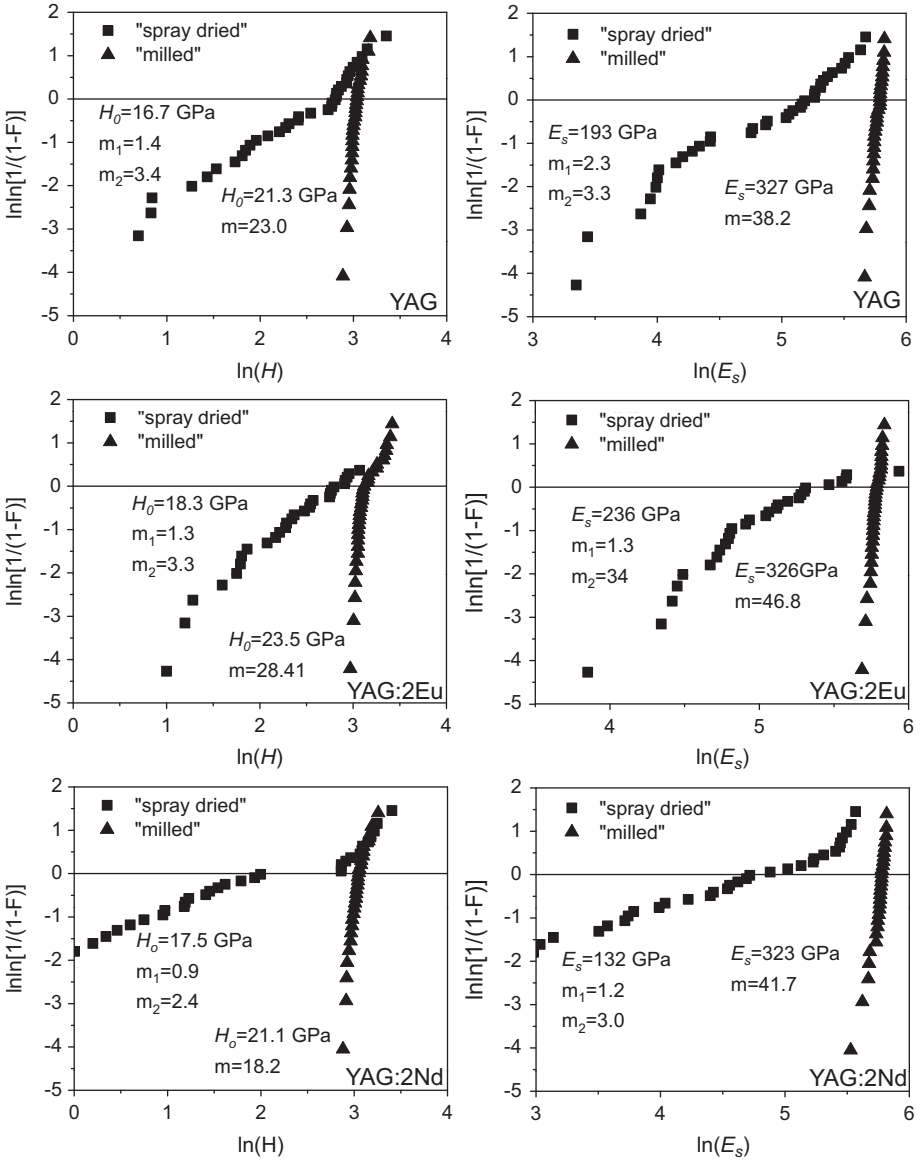

Fig. 7. Weibull dispersion analysis of hardness and Young's modulus of doped and undoped "spray dried" and "milled" YAG samples.

YAG fibers, as opposed to dense samples, but with the same type and concentration of dopants [25]. Overall, the hardness and stiffness values of the amorphous fibers are low compared to the values obtained for the crystalline YAG compacts investigated in this work. For example, the hardness and stiffness of pure amorphous YAG fibers are less than 30% of the values determined for the corresponding crystalline sample. Interestingly, for the amorphous YAG fibers, a positive effect of Nd additions on the mechanical properties was observed.

4. Conclusions

The use of a modified version of the Pechini-type precursor method based on spray drying and an additional step of milling allowed the preparation of highly dense doped YAG ceramics sintered at 1,550 °C in air. A small increase in the lattice parameter due to Eu and Nd additions was measured, as expected, but no measurable effects on the mechanical properties were observed. Comparison with previous reports of the mechanical performance of amorphous fibers showed that the polycrystalline samples produced in this study achieved more than twice the values obtained with the best amorphous fibers. Thus, the use of amorphous fibers produced by the melt extraction method as a reinforcing agent is limited by their mechanical performance, and the YAG polycrystalline materials produced as described in this paper are better candidates to be used as reinforcing agents for high temperature applications.

References

[1] T.A. Parthasarathy, T.I. Mah, L.E. Matson, Processing, structure and properties of alumina-YAG eutectic composites, Journal of Ceramic Processing Research 5 (2004) 380–390.

[2] M. Jimenez-Melendo, H. Haneda, H. Nozawa, Ytterbium cation diffusion in yttrium aluminum garnet (YAG)-implications for creep mechanisms, Journal of the American Ceramic Society 84 (2001) 2356–2360.
[3] T.A. Parthasarathy, T.I. Mah, L.E. Matson, Deformation behavior of an Al2O3–Y3Al5O12 eutectic composite in comparison with sapphire and YAG, Journal of the American Ceramic Society 76 (1993) 29–32.
[4] X. Li, H. Liu, J. Wang, H. Cui, F. Han, YAG:Ce nano-sized phosphor particles prepared by a solvothermal method, Materials Research Bulletin 39 (2004) 1923–1930.
[5] Y. Waku, N. Nakagawa, H. Ohtsubo, A. Mitani, K. Shimizu, Fracture and deformation behaviour of melt growth composites at very high temperatures, Journal of Materials Science 36 (2001) 1585–1594.
[6] S. Deng, R. Warren, Creep properties of single crystal oxides evaluated by a Larson–Miller procedure, Journal of the European Ceramic Society 15 (1995) 513–520.
[7] T.A. Parthasarathy, T.I. Mah, K. Keller, Creep mechanism of polycrystalline yttrium aluminum garnet, Journal of the American Ceramic Society 75 (1992) 1756–1759.
[8] S. Karato, Z. Wang, K. Fujino, High-temperature creep of yttrium–aluminium garnet single crystals, Journal of Materials Science 29 (1994) 6458–6462.
[9] G.N. Morscher, K.C. Chen, K.S. Mazdiyasni, Creep-resistance of developmental polycrystalline yttrium-aluminum garnet fibers, Ceramic Engineering and Science Proceedings 15 (1994) 181–188.
[10] P. Apte, H. Burke, H. Pickup, Synthesis of yttrium aluminum garnet by reverse strike precipitation, Journal of Materials Research 7 (1992) 706–711.
[11] S.M. Sim, Characterization of spray-dried yttrium aluminum garnet powder, Journal of the Korean Ceramic Society 1 (1995) 35–39.
[12] J.G. Li, T. Ikegami, J.H. Lee, T. Mori, Low-temperature fabrication of transparent yttrium aluminum garnet (YAG) ceramics without additives, Journal of the American Ceramic Society 83 (2000) 961–963.
[13] G. Gowda, Synthesis of yttrium aluminates by the sol-gel process, J, Materials Science Letters 5 (1986) 1029–1032.
[14] S.M. Sim, K.A. Keller, T.I. Mah, Phase formation in yttrium aluminum garnet powders synthesized by chemical methods, Journal of Materials Science 35 (2000) 713–717.
[15] T. Tachiwaki, M. Yoshinaka, K. Hirota, T. Ikegami, O. Yamaguchi, Novel synthesis of Y3Al5O12 (YAG) leading to transparent ceramics, Solid State Communications 119 (2001) 603–606.
[16] N. Matsushita, N. Tsuchiya, K. Nakatsuka, T. Yanagitani, Precipitation and calcination processes for yttrium aluminum garnet precursors synthesized by the urea method, Journal of the American Ceramic Society 82 (1999) 1977–1984.
[17] M. Nyman, J. Caruso, M.J. Hampden-Smith, T.T. Kodas, Comparison of solid-state and spray-pyrolysis synthesis of yttrium aluminate powders, Journal of the American Ceramic Society 80 (1997) 1231–1238.
[18] S. Roy, L. Wang, W. Sigmund, F. Aldinger, Synthesis of YAG phase by a citrate–nitrate combustion technique, Materials Letters 39 (1999) 138–141.
[19] B.J. Chung, J.Y. Park, S.M. Sim, Synthesis of yttrium aluminium garnet powder by a citrate gel method, Journal of Ceramic Processing Research 4 (2003) 145–150.
[20] J. Zarate, R. Lopez, E.A. Aguilar, Synthesis of yttrium aluminum garnet by modifying the citrate precursor method, Advances in Technology of Materials and Materials Processing Journal 7 (2005) 53–56.
[21] M.K. Cinibulk, Synthesis of yttrium aluminum garnet from a mixed-metal citrate precursor, Journal of the American Ceramic Society 83 (2000) 1276–1278.
[22] Y. Liu, L. Gao, Low-temperature synthesis of nanocrystalline yttrium aluminum garnet powder using triethanolamine, Journal of the American Ceramic Society 86 (2003) 1651–1653.
[23] A.C. Fischer-Cripps, Nanoindentation, Springer-Verlag, New York, 2002.
[24] W.C. Oliver, G.M. Pharr, An improved technique for determining hardness and elastic modulus using load and displacement sensing indentation experiments, Journal of Materials Research 7 (1992) 1564–1583.
[25] R. Lopez, E.A. Aguilar, J. Zarate-Medina, J. Muñoz-Saldana, D. Lozano-Mandujano, Nanoindentation of melt-extracted amorphous YAG and YAG:Eu, Nd micrometric fibers synthesized by the citrate precursor method, Journal of the European Ceramic Society 30 (2010) 73–79.
[26] S. Bhattacharyya, T.K. Mukhopadhyay, K. Dana, S. Ghatak, Pressureless reaction sintering of yttrium aluminium garnet (YAG) from powder precursor in the hydroxyhydrogel form, Ceramics International 37 (2011) 3463–3468.
[27] M.L. Saladino, E. Caponetti, D. Chillura Martino, S. Enzo, G. Ibba, Effect of the dopant selection (Er, Eu, Nd or Ce) and its quantity on the formation of yttrium aluminum garnet nanopowders, Optical Materials 31 (2008) 261–267.
[28] D. Klimm, S. Ganschow, A. Paj″aczkowska, L. Lipińska, On the solubility of Nd^{3+} in $Y_3Al_5O_{12}$, Journal of Alloys and Compounds 436 (2007) 204–208.
[29] H. Hertz, On the contact of elastic solids, Journal Fur Die Reine Und Angewandte Mathematik 92 (1882) 156–171.
[30] H. Yagi, T. Yanagitani, T. Numazawa, K. Ueda, The physical properties of transparent Y3Al5O12: elastic modulus at high temperature and thermal conductivity at low temperature, Ceramics International 33 (2007) 711–714.
[31] C. Lu, R. Danzer, F.D. Fischer, Fracture statistics of brittle materials: Weibull or normal distribution, Physical Review E 65 (2002) 1–4.
[32] D.R. Askeland, P.P. Fulay, Essentials of Materials Science and Engineering, Cengage Learning, Stanford, 2009.